

Nanolithography using molecular optics

Robert J. Gordon^{a)} and Langchi Zhu

Department of Chemistry (m/c 111), University of Illinois at Chicago, 845 West Taylor Street, Chicago, Illinois 60607-7061

W. Andreas Schroeder

Department of Physics (m/c 273), University of Illinois at Chicago, 845 West Taylor Street, Chicago, Illinois 60607-7059

Tamar Seideman

Department of Chemistry, Northwestern University, 2145 Sheridan Road, Evanston, Illinois 60208-3113

(Received 12 February 2003; accepted 4 April 2003)

We explore the possibility of using an intense laser beam to focus a molecular beam onto a surface to create nanowires. We show that with a grazing angle of incidence between the laser and molecular beams, it is possible to use available technology to create wires < 50 nm wide and > 100 μm long with a 100 W continuous wave laser. Narrower and longer features could be created with higher power lasers. This technique is very general, and may be used to deposit any atom or molecule onto an arbitrary substrate, so long as the particles may be entrained in a molecular beam and have an adequate sticking probability. The effects of spherical and chromatic aberration and laser mode structure on the focusing properties of the molecular lens are examined in detail, and design criteria for building a practical device are discussed. © 2003 American Institute of Physics.

[DOI: 10.1063/1.1578173]

I. INTRODUCTION

Theoretical¹⁻⁵ and experimental⁶⁻⁹ studies over the past few years have shown that it is possible to use intense laser fields to manipulate the center-of-mass motion of molecules. Molecular deflection, focusing and dispersion have been realized in the laboratory, and a recent theoretical study extended the field of molecular optics to include molecular mirrors.⁵ Theoretical work has also indicated the possibility of fabricating molecular wires of nanometer-scale width by focusing a molecular beam onto a surface.¹ Several formal problems associated with creating such structures were studied,⁴ but an experimental realization has not been reported as yet. The objective of this article is to explore the feasibility of building a nanolithography device that utilizes the principles of molecular optics.

The underlying principle of molecular optics is the interaction of the spatially inhomogeneous electric field of a laser beam with the molecular polarizability tensor. The field-matter interaction at nonresonant frequencies, for a linearly polarized electric field and a linear or symmetric top molecule, can be cast in the form of an induced Hamiltonian (see Ref. 5)

$$H_{\text{ind}}(r, \Theta, t) = -\frac{1}{4} \varepsilon^2(r, t) (\alpha_{\parallel} \cos^2 \Theta + \alpha_{\perp} \sin^2 \Theta), \quad (1)$$

where $E(r, t) = \varepsilon(r, t) \cos \omega_l t$ is the electric field, ω_l is the laser frequency, Θ is the angle between the polarization vector and the molecular axis, and α_{\parallel} and α_{\perp} are the components of the polarizability tensor parallel and perpendicular

to the molecular axis, respectively. In the case of laser radiation with a circular Gaussian spatial profile, the field is given by

$$\varepsilon(r, t) = \varepsilon_0 \hat{\varepsilon} e^{-r^2/\omega^2} f(t), \quad (2)$$

where ε_0 is the peak amplitude of the field, ω is its 1/e radius, $f(t)$ is its temporal envelope, and $\hat{\varepsilon}$ is a unit vector in the polarization direction. The radial gradient of the potential energy generates a force that may deflect the molecule, whereas the angular gradient induces a torque that may align the molecule along $\hat{\varepsilon}$.⁵ The well depth of the time-averaged radial potential may be hundreds of K deep, as compared with the μK well depths typically encountered in optical lattices used to trap atoms.¹⁰ A rough estimate of the laser-induced well depth, $V_w^{J|M|}$, for the $J=0$, $M=0$ rotational state is $V_w^{00} = 15 \alpha_{\parallel} I_0 \text{K}$, where α_{\parallel} is in \AA^3 and the peak intensity, I_0 , is in TW/cm^2 .

A focused laser beam behaves like a “molecular lens” that can squeeze a molecular beam into a narrow stripe. Molecular focusing is illustrated schematically in Fig. 1, where the laser propagates along the x axis, and the laser and molecular beams intersect in the xz plane. Panel (a) is drawn in the plane of the two beams, which intersect at an angle δ . The target surface is perpendicular to this plane and is parallel to the laser beam. Panel (b) is drawn in a plane perpendicular to the target and the laser beam, and shows a cross section of the laser focal spot. The molecular beam propagates from the right, below the plane of the page (unless $\delta = 90^\circ$, in which case it propagates in the plane of the page), intersects the laser beam waist, and reaches the target above the plane of the page. Two schematic trajectories illustrate focusing of the molecular beam onto the surface. Panel (c)

^{a)} Author to whom correspondence should be addressed; electronic mail: rjgordon@uic.edu

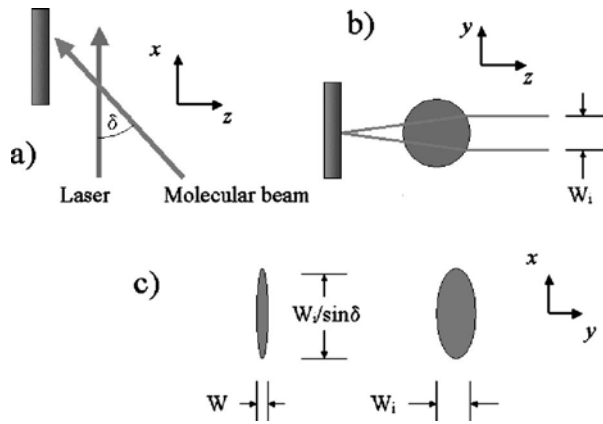


FIG. 1. Schematic drawing of the focusing of a molecular beam by a laser beam, shown from three orthogonal perspectives: (a) Plane of the two beams: The laser propagates in the x direction, and the molecular beam intersects it at angle, δ . (b) Plane perpendicular to the laser beam: The initial width of the molecular beam is W_i . (c) Plane containing the target surface, parallel to the laser beam. The width of the focused molecular beam is W . The target surface is shown on the left of panels (a) and (b).

shows slices of the molecular beam in planes parallel to the target surface. The slice on the right shows the molecular beam before it is focused by the laser, having a collimated width W_i . The aspect ratio of this cross section is determined by the angle of incidence to the target. The slice on the right shows the focused molecular beam. It is readily seen that the molecular beam is compressed so as to have an elliptical cross section in the xy plane with its major axis along the y direction.

For later reference it is useful to summarize the qualitative features that are general to molecular lenses (independent of the molecule and field parameters). It has been shown^{2,3} that the lens parameters scale with the ratio $R = E_{\text{kin}z} / V_w^{J|M|}$ between the component of the kinetic energy transverse to the laser beam and the laser-induced well depth. The energy ratio characterizes the molecular lens in much the same way that the refractive index determines the properties of an optical lens. The focal distance is essentially linear in R except in the small- R limit, whereas the image size is constant in R for large values of the energy ratio, dropping rapidly as R decreases below ~ 3 .

In its original conception,¹⁻³ molecular optics was formulated with the laser and molecular beams perpendicular to each other [i.e., with $\delta = 90^\circ$ in Fig. 1(a)], and experimental realizations⁶⁻⁹ have so far been confined to this geometry. In these studies the laser beam was pulsed in order to obtain sufficient intensity. Here we show that, for the purpose of nanolithography, a grazing angle of incidence between the laser and molecular beams may offer a number of significant advantages. At grazing incidence, the energy ratio $R \propto v_z^2 / I_0$ (where $v_z = v \sin \delta$ is the z component of the velocity, and I_0 is the peak intensity) for a given intensity is dramatically reduced as compared to the perpendicular configuration. Equivalently, for the value of R required to achieve a desired focal distance, the requisite laser intensity is drastically reduced. This reduction in the intensity opens the opportunity of employing continuous-wave (cw) laser technology to focus molecular beams. The use of a cw laser would increase

the write rate by many orders of magnitude as compared to a low-duty-cycle pulsed source.

The use of a cw radiation source also eliminates the problem of background molecules accumulating on the surface when the laser is off. In principle, unwanted collisions with the surface may be suppressed also with a pulsed source, either by employing molecular and laser pulses of comparable duration or by splitting the laser into several components, so that one serves to deflect and another to focus the molecular beam. In practice, however, both routes would be difficult to implement.

In this article, we examine the properties of the laser and molecular beams needed for constructing a nanolithography apparatus. In particular, we explore the properties of a molecular lens using a cw laser beam at a variable incidence angle. In the following section we describe the computational methods. In Sec. III we investigate the effects of the incidence angle, the laser intensity, focal radius and mode structure, the translational and rotational temperatures of the molecular beam, and the polarizability anisotropy of the molecule. In Sec. IV, we discuss several aspects of the laser and molecular beam design involved in constructing a practical apparatus, and in Sec. V we summarize our conclusions.

II. COMPUTATIONAL METHODS

We employ in this study the semiclassical methods developed in Ref. 2 to calculate the trajectories of a collimated molecular beam interacting with a focused laser beam. Following adiabatic separation of the center of mass from the internal modes, the rotational problem is solved quantum mechanically by diagonalizing the complete Hamiltonian at fixed values of the laser field

$$[H_{\text{rot}} + H_{\text{ind}}(\epsilon)]|JM;\epsilon\rangle = E^{J|M|}(\epsilon)|JM;\epsilon\rangle. \quad (3)$$

Here H_{rot} is the free rotor Hamiltonian, and $H_{\text{ind}} = -1/4\epsilon^2[\alpha_{\perp} + (\alpha_{\parallel} - \alpha_{\perp})\cos^2\Theta]$ is the induced Hamiltonian of Eq. (1). The eigenstates $|JM;\epsilon\rangle$ are expanded in a basis set of field-free rotor states with ϵ -dependent expansion coefficients, determined by solving the eigenvalue problem (3). The eigenvalues $E^{J|M|}(\epsilon)$ serve as adiabatic potentials for propagation of the center-of-mass motion. Taking into account the divergence of the laser beam, the amplitude of an elliptical Gaussian field with a wavelength λ and a TEM₀₀ mode is given by¹¹

$$\epsilon(x, y, z) = \epsilon_0 \left(\frac{\omega_{0y}\omega_{0z}}{\omega_y(x)\omega_z(x)} \right)^{1/2} e^{-\{y^2/\omega_y^2(x) + z^2/\omega_z^2(x)\}}, \quad (4)$$

where

$$\omega_y^2 = \omega_{0y}^2 + \theta_y^2 x^2, \quad \omega_z^2 = \omega_{0z}^2 + \theta_z^2 x^2, \quad (5)$$

and the divergence angles are given by

$$\theta_{y(z)} = \frac{\lambda}{\pi\omega_{0y(0z)}}. \quad (6)$$

The origin of the coordinate system is taken to be the focal point of the field (see Fig. 1).

Having computed quantum mechanically the effective potentials for the center-of-mass motion subject to the inho-

homogeneous electric field, we proceed to describe the corresponding dynamics by numerical integration of Hamilton's equations of motion^{2,3}

$$\dot{x} = \frac{p_x}{m}, \quad \dot{p}_x = -\frac{\partial E^{J_i|M|}[\varepsilon(x, y, z)]}{\partial x}, \quad (7a)$$

$$\dot{y} = \frac{p_y}{m}, \quad \dot{p}_y = -\frac{\partial E^{J_i|M|}[\varepsilon(x, y, z)]}{\partial y}, \quad (7b)$$

$$\dot{z} = \frac{p_z}{m}, \quad \dot{p}_z = -\frac{\partial E^{J_i|M|}[\varepsilon(x, y, z)]}{\partial z}. \quad (7c)$$

The initial coordinates, x_0 , y_0 , and z_0 , are selected as follows. The molecular beam is assumed to have a nondiverging square cross section of width W_i , and n_y values of y_0 are selected uniformly between the limits $-W_i/2$ and $W_i/2$. The initial values of x and z are given by

$$x_0 = r_s \cos \delta + \rho \sin \delta, \quad z_0 = r_s \sin \delta + \rho \cos \delta, \quad (8)$$

where the ‘‘shell’’ radius r_s is the distance from the center of the cross section of the molecular beam to the focal point of the laser, and ρ is the distance along a line perpendicular to the line of centers in the xz plane. The value of r_s is chosen large enough that a further increase in the shell radius does not affect the focal properties of the lens; ρ is selected uniformly between $-W_i/2$ and $W_i/2$.

The speed of the molecules is assumed to have a supersonic Maxwellian distribution for a seed gas of mass m mixed with a carrier gas of mass m_c with translational temperature T_{trans} . For a highly dilute gas with no velocity slippage, the speed distribution function of the seed gas is given by¹²

$$g(v) = (1/q_{\text{trans}}) v^2 e^{-\left(\frac{v-v_f}{\alpha}\right)^2}, \quad (9)$$

where q_{trans} is a normalization constant, $\alpha = (2kT_{\text{trans}}/m)^{1/2}$ is the most-probable speed of the seed gas in the moving frame, and the flow speed is given by

$$v_f = v_\infty \left(1 - \frac{T}{T_0}\right)^{1/2}. \quad (10)$$

The speed of the carrier gas at infinite Mach number is given by

$$v_\infty = \left(\frac{\gamma_c}{\gamma_c - 1}\right)^{1/2} \alpha_{0c}, \quad (11)$$

where γ_c is the heat capacity ratio, T_0 , is the stagnation temperature, and $\alpha_{0c} = (2kT_0/m_c)^{1/2}$. For an arbitrary incidence angle, the initial velocity components are given by

$$v_{0x} = v \cos \delta, \quad v_{0y} = 0, \quad v_{0z} = v \sin \delta. \quad (12)$$

The properties of the molecular lens that are of greatest interest are the width, W , of the molecular beam at the focal waist (i.e., the image size of the molecular lens) and the coordinates of the focal waist, x_f and z_f . (See Fig. 1 of Ref. 3 for definitions of the lens parameters.) We determine the former by evaluating $y(t)$ as a function of $z(t)$, averaged over all initial conditions. This quantity is given by

$$\langle y(z) \rangle = \frac{1}{n_y n_\rho} \sum_J \sum_{|M|=0}^J \sum_{i=1}^{n_y} \sum_{j=1}^{n_\rho} \sum_k g(v_k; T_{\text{trans}}) \times \Delta v P_{J,|M|} y(t; y_{0,i}, \rho_j), \quad (13)$$

where Δv is the spacing of grid points in the speed distribution, and $P_{J,|M|}$ is the Boltzmann rotational population. The focal width, W , is computed as the minimum of $\langle y[z(t)] \rangle$, which occurs at $t = t_f$, and the focal coordinates are the resulting values of $x(t_f)$ and $z(t_f)$.

III. RESULTS

Molecules with different initial conditions intersect the xz plane at different locations, resulting in a nonzero width of the focused structure. It is logical therefore first to inquire which physical properties of the molecular and laser beams determine the coordinates of the molecular beam waist, and then to investigate the conditions needed for minimizing the focal width, while maintaining a useful focal distance.

The regime of interest to the present work is the large- R limit, where the focal distance is linear in R and the width parameter is R independent.³ In this limit, the location of the focus is determined by the intensity and velocity, and the width is determined by spherical and chromatic aberrations. Specifically, the calculations presented here confirm that the focal coordinates scale as

$$x_f, z_f \sim m \omega_0 T_0 / m_c \alpha_{\parallel} I_0. \quad (14)$$

The calculations reported here were performed using I_2 as a prototypical molecule, with $\alpha_{\parallel} = 17 \text{ \AA}^3$ and $\alpha_{\perp} = 8 \text{ \AA}^3$, and Xe as the carrier gas with $T_0 = 300 \text{ K}$. Because the focal coordinates vary inversely with the product $m_c I_0$, the calculations apply equally to any carrier gas with the intensity appropriately scaled. The initial width of the molecular beam was set at $W_i = 10 \mu\text{m}$ with $n_y = 40$, and the electric field radius was usually set at $30 \mu\text{m}$. Because averaging over ρ did not affect the focal parameters significantly, we typically set $n_\rho = 1$.

A. Focal coordinates

The quantities that are most important in determining the location of the focus of the molecular beam are the laser intensity and spot size, the molecular speed, and the incidence angle. Figure 2 confirms that for large R both x_f and z_f vary inversely with laser intensity, and similar calculations verified the mass and polarizability scaling of Eq. (14).³ We also found that the focal coordinates for a given intensity depend on the lens curvature, increasing linearly with $\omega(x)$ for a circular Gaussian beam. (The properties of a molecular lens based on an elliptical optical focus are discussed in Sec. III B).

Perhaps the most interesting result is the dependence of x_f and z_f on the intersection angle of the beams, shown in Fig. 3. We find that z_f decreases with δ , falling to zero at grazing incidence. This result is expected because v_z , the component of the velocity transverse to the laser beam, decreases with δ . Also, as expected, x_f initially increases with angle, tracking the corresponding increase of v_x . A less intuitive result is that $x_f = z_f$ at 45° and decreases monotonically

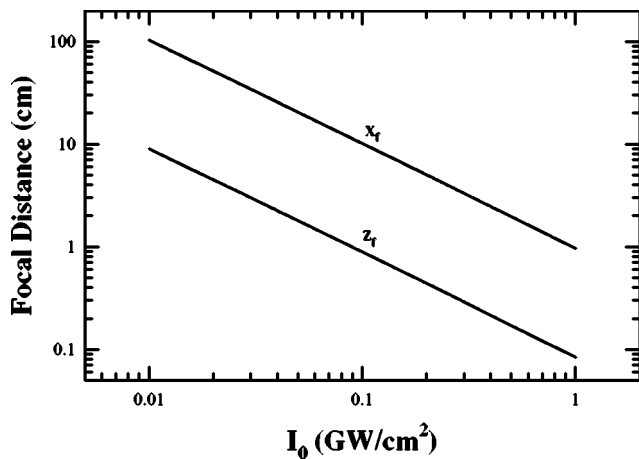


FIG. 2. Intensity dependence of the focal coordinates in the large- R limit. The calculations were performed for I_2 in a Xe carrier gas at an incidence angle of $\delta=5^\circ$. The range of the energy ratio, R , is 43–4300.

cally at larger angles. An examination of individual trajectories reveals the physical basis for this behavior. As a molecule traverses the laser beam it feels a time-dependent force. As v_z decreases, the magnitude of the associated impulse increases, resulting in smaller values for both x_f and z_f . The maximum in x_f reflects the competition between increasing transverse velocity and increasing impulse. It is this property that makes it possible to use a continuous laser for lithography.

B. Focal width

In this section, we investigate the effects of spherical and chromatic aberrations on the focal width. In these calculations, we set $\delta=5^\circ$ and $I_0=10^8$ W/cm², noting that other values of these parameters yield essentially the same values of W (because we consider here the large R regime).

Figure 4(a) shows a set of trajectories for a monoenergetic beam of I_2 molecules (with $T_{\text{trans}}=T_{\text{rot}}=0$) and a circular laser focus ($\omega_0=\omega_{0y}=\omega_{0z}=30$ μm). The width of the molecular focus is caused by spherical aberration of the

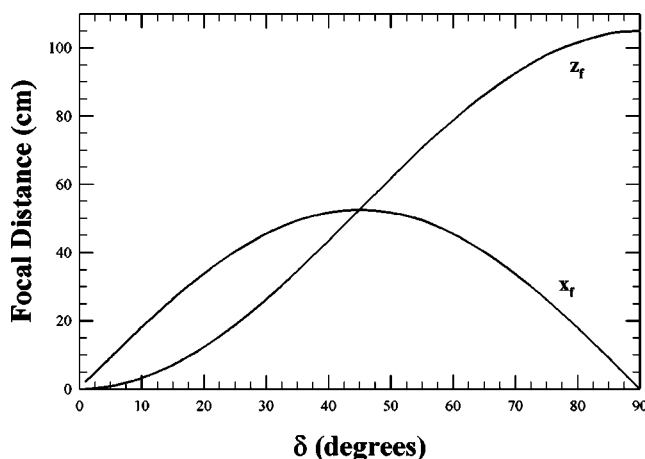


FIG. 3. Focal coordinates of the molecular beam as a function of incidence angle. The calculations were performed for a beam of I_2 in Xe at a laser intensity of 10^8 W/cm².

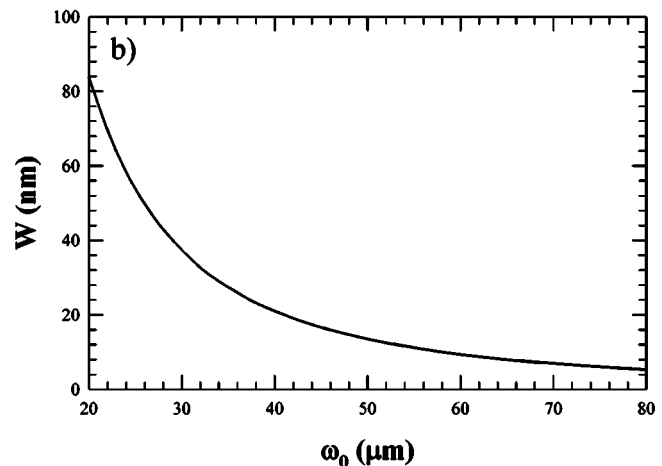
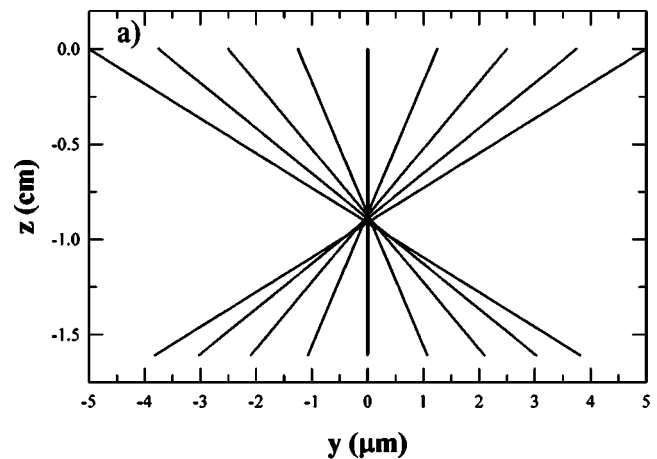


FIG. 4. The effect of spherical aberration on the focal width of the molecular beam. (a) Trajectories for a molecular beam of I_2 in Xe having an initial width $W_i=10$ μm focused by a laser with $\omega_0=30$ μm , at a peak intensity of 10^8 W/cm² and an intersection angle of 5° . Both the translational and rotational temperatures are zero. (b) Variation of the focal width with the radius of a circular Gaussian focus.

electromagnetic lens. Figure 4(b) shows that this effect may be remedied by increasing ω_0 . Under the conditions of these calculations, W varies as W_i/ω_0^2 , falling to 5 nm for $\omega_0=80$ μm . This effect has a simple origin that was noted previously.³ Spherical aberration arises from the anharmonic shape of the potential that governs the trajectories. For a fixed molecular beam diameter, the molecules feel an increasingly harmonic force field as the spot size of the laser in the direction transverse to the plane of the molecular and laser beams [see Fig. 1(b)] is increased.

In the small R regime, the use of an elliptical focus is advantageous, because it reduces the laser power while at constant intensity, with the additional benefit of increasing the focal distance. Calculations with an elliptical focus in the large R limit show that, as expected, the focal width for a constant intensity depends only on ω_y . For an elliptical beam with $\omega_z < \omega_y$, the laser power required to produce a particular focal width decreases with ω_z . The calculations also show, however, that the focal distance for an elliptical beam is greater than for a circular beam with the same ω_y . In the large- R regime, ellipticity presents no advantage, because a greater focal distance is undesirable. In that case the

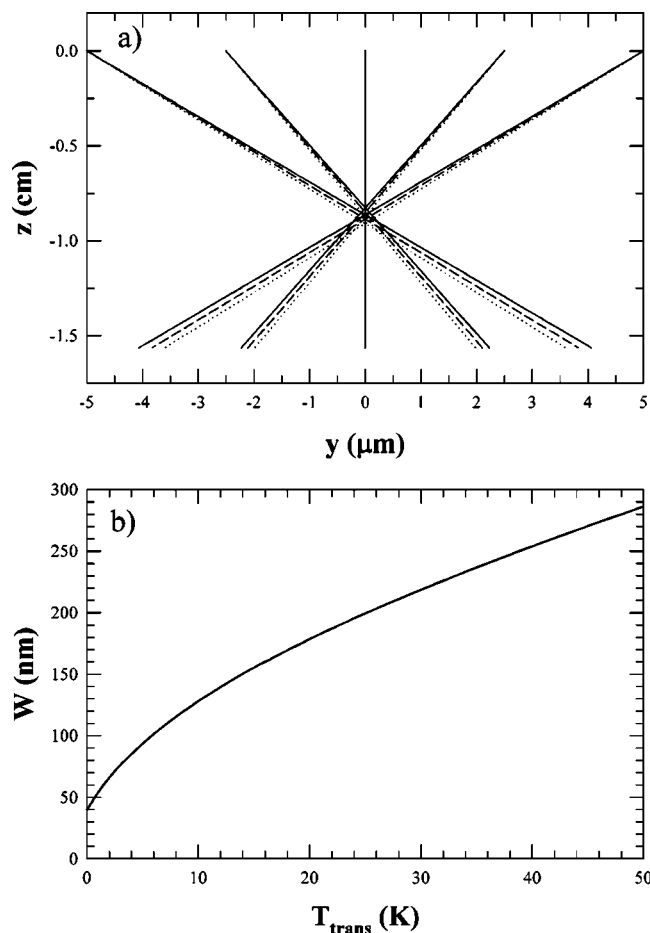


FIG. 5. Chromatic aberration produced by the translational energy distribution of the molecular beam. (a) Trajectories for a molecular beam of I_2 in a Xe carrier gas with $T_{\text{trans}}=1$ K. The three trajectories for each value of y_0 are for speeds equal to $v_{\text{mp}}+\alpha$ (solid lines), v_{mp} (dashed lines), and $v_{\text{mp}}-\alpha$ (dotted lines), where v_{mp} is at the most probable speed. (b) Focal width as a function of the translational temperature. The other physical parameters are as in Fig. 4.

higher intensity required to offset the increased focal distance cancels the savings in laser power that might otherwise have been achieved.

One source of chromatic aberration is the spread in initial speed of the molecular beam. Molecules with larger values of R are deflected less during their passage through the laser beam and, therefore, come to a focus at larger distances [see Fig. 5(a)]. Consequently, the ensemble averaged image size is larger than for monochromatic trajectories. Clearly, $\langle y \rangle$ increases with T_{trans} , as shown in Fig. 5(b). For the case of iodine molecules we find at a translational temperature $T_{\text{trans}}=1$ K (which is readily achieved in a supersonic molecular beam) an image size of 54 nm, as compared to the monochromatic value of 38 nm.

A second source of chromatic aberration is the rotational temperature of the molecular beam. The force felt by a diatomic molecule depends on the direction of the angular momentum vector, \mathbf{J} . If the molecule rotates in a plane perpendicular to \mathbf{J} (i.e., if $|M|=J$), it feels a smaller force than if it rotates in a plane containing \mathbf{J} (i.e., $M=0$). As shown in Fig. 6(a), the focal distance is very sensitive to J and $|M|$, so that, although each rotational state comes to a sharp focus, the

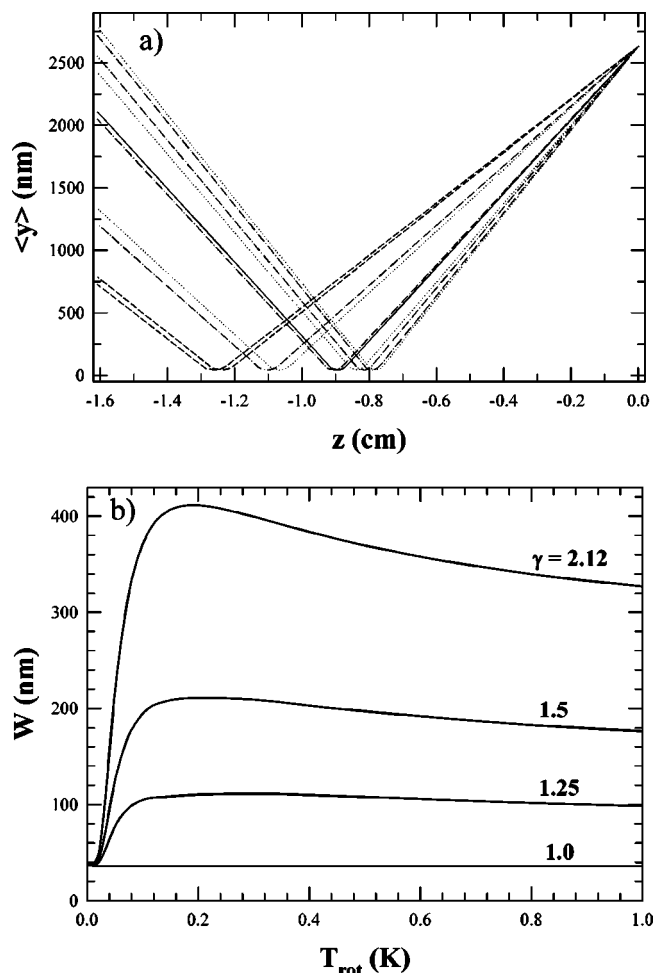


FIG. 6. Chromatic aberration produced by rotational temperature. (a) Local width of the molecular beam as a function of the transverse distance for different free rotor states. Shown here are the evolution of $\langle y \rangle$ for $J=0$ (solid curve), $J=1$ (dashed), $J=2$ (dotted), and $J=3$ (dot-dashed). For $J=2$ and 3, the value of $|M|$ increases from 0 to J starting from the lowest curve. For $J=0$ the order of the M curves is reversed. (b) The focal width, summed over all rotational states, as a function of rotational temperature. The curves are for different values of the ratio of $\gamma = \alpha_{\parallel}/\alpha_{\perp}$, with $\gamma = 2.12$ corresponding to I_2 molecules. The calculations were performed assuming $T_{\text{trans}}=0$. The other physical parameters are as in Fig. 4.

sum of over all J, M states results in a considerably broadened beam waist. The dependence of W on T_{rot} is shown in Fig. 6(b). The maximum near 0.2 K occurs because $J=0$ and $J=1$ differ the most in their focal distances, and at this temperature these states have approximately equal populations. At higher T_{rot} the focal points are distributed over many more states, and the focal width slowly declines with temperature.

The effect of rotational alignment depends on the anisotropy of the polarizability. To study this dependence we artificially varied the ratio of polarizability components, $\gamma = \alpha_{\parallel}/\alpha_{\perp}$, which for I_2 has a value of 2.12. Figure 6(b) shows that, as expected, W decreases with γ , and for spherically symmetric molecules it is independent of T_{rot} .

C. Effects of laser mode structure

In the previous calculations we assumed a TEM_{00} Gaussian mode. We expect, however, that the focusing prop-

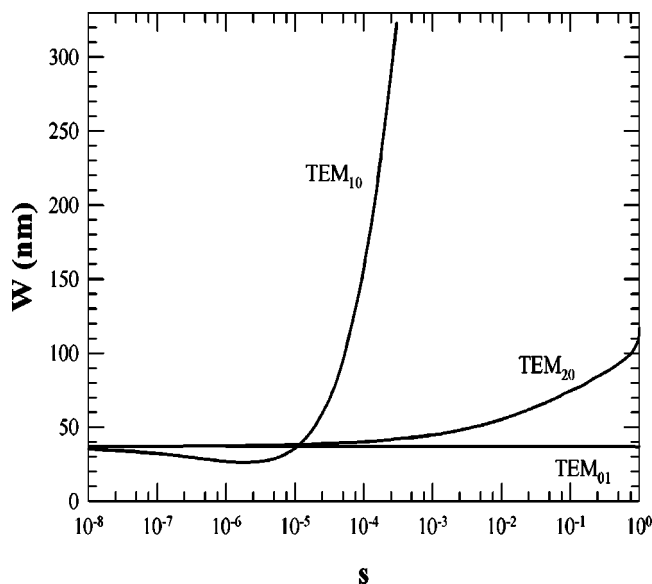


FIG. 7. The effect of Gaussian laser transverse mode structure on the focal width. The parameter s is the fraction of the laser intensity in the higher order mode. All other physical parameters are as in Fig. 4.

erties of a molecular lens would be very sensitive to the transverse mode structure of the laser beam. In particular, we anticipate that the presence of a node in the center of the beam would have a large effect. The electric field for a circular Gaussian beam with a TEM_{mn} mode is given by¹¹

$$E_{mn} = E_{0,mn} \frac{\omega_0}{\omega(x)} H_m \left(\sqrt{2} \frac{y}{\omega(x)} \right) H_n \left(\sqrt{2} \frac{z}{\omega(x)} \right) \times \exp \left(-\frac{y^2 + z^2}{\omega^2(x)} + i\alpha_0 + i(m+n)\eta(x) \right), \quad (15)$$

where H_j is a Hermite polynomial of order j , $E_{0,mn}$ is the amplitude of the field, α_0 is the spatially dependent phase of the TEM_{00} mode, and

$$\eta(x) = \cos^{-1} \left(\frac{\omega_0}{\omega(x)} \right). \quad (16)$$

In order to evaluate the effects of individual laser modes on the properties of a molecular lens, we calculated W for a field consisting of a superposition of TEM_{00} and the mode of interest

$$E = \sqrt{1-s} E_{00} + \sqrt{s} E_{mn}, \quad (17)$$

where s is the fractional intensity in the higher order mode. The results for TEM_{01} , TEM_{10} , and TEM_{20} are shown in Fig. 7 as a function of s . Not surprisingly, the TEM_{01} mode, which is symmetric with respect to the z axis, has no effect on the focal distance (just as W does not depend on ω_z for an elliptical TEM_{00} mode). The TEM_{10} mode, on the other hand, has a very strong effect. For small values of s , the extended intensity along the y axis actually improves the focusing, with the bimodal field acting like an achromatic lens. For intensity ratios $> 10^{-5}$, however, the central node strongly defocuses the molecular beam. The TEM_{20} mode, which has a maximum at $y=0$, has a much smaller defocusing effect at all s .

From these calculations it is clear that even a small intensity in some of the higher order modes can have a deleterious effect. Although the amplitudes of these modes may be suppressed by spatial filtering, a small residual contribution could be troublesome. An efficient way of completely suppressing the unwanted modes is to pass the laser beam through a capillary, producing an electromagnetic field having the form of a truncated Bessel function (the fundamental EH_{mn} of the guide¹³)

$$E_b = E_{0,b} J_0 \left(\rho_0 \frac{r}{a} \right), \text{ for } r \leq a \quad (18a)$$

$$= 0 \text{ for } r > a, \quad (18b)$$

where a is the radius of the capillary, $r = (y^2 + z^2)^{1/2}$, and $\rho_0 = 2.4048$ is the first zero of the zero-order Bessel function, J_0 .¹⁴

We find that this field has superior focusing properties to the TEM_{00} Gaussian field. Choosing $a = \omega_0$ and $E_{0,b} = E_{0,00}$, with equal laser intensity, the Bessel beam produces a slightly larger focal width (45 vs 38 nm at $a = 30 \mu\text{m}$ and $I_0 = 1 \times 10^8 \text{ W/cm}^2$) at a slightly shorter focal distance ($x_f = 8.4 \text{ cm}$ and $z_f = 0.73 \text{ cm}$ vs. 9.2 and 0.81 cm at $\delta = 5^\circ$). Increasing a to $40.86 \mu\text{m}$, so that the laser power for the Bessel beam is the same as for a Gaussian beam with $\omega_0 = 30 \mu\text{m}$, reduces W to 25 nm and increases the focal distances to 11.2 and 0.98 cm. The most important property of the Bessel field, however, is that its decomposition into transverse resonator modes requires cylindrically symmetric Laguerre–Gaussian modes, which do not defocus the molecular beam.

IV. DESIGN CONSIDERATIONS

In this section, we discuss the key properties of the molecular and laser beams that would be needed for constructing a practical lithography apparatus.

The molecular beam must have sufficient intensity to have a useful write rate, and it must be sufficiently well collimated to deposit wires of the desired width. The number of particles hitting the target surface per unit time is given by $\Phi F \Omega$, where Φ is the total initial particle flux, F is the mole fraction of the seed gas, and Ω is the solid angle of the final aperture. The write rate is then

$$\Gamma = \Phi F \Omega \sigma P_s / A, \quad (19)$$

where A is the feature area, σ is the collision cross section of the molecule, and P_s is its sticking probability. For $\Phi = 10^{19} \text{ sr}^{-1} \text{ s}^{-1}$,^{15,16} $F = 1\%$, and $P_s = 10\%$, with a $10\text{-}\mu\text{m}$ -diam collimating aperture located at a distance of 1 m from the beam source, a feature size of $50 \text{ nm} \times 100 \mu\text{m}$, and $\sigma = 1 \text{ nm}^2$, the write rate is 0.1 ML/s. A pointing stability of the molecular beam of 20 nm, which is normally achieved in an atom interferometer,¹⁵ could be obtained by attaching the collimating apertures to piezoelectric transducers driven by a feedback signal provided by a laser interferometer.

In selecting the operating conditions of the molecular beam, one must consider possible trade-offs between particle flux, peak velocity, and translational temperature (i.e., width of the speed distribution), all of which may be affected by

condensation of the carrier gas. The rate of cluster formation varies as $d^a P^b$, where d is the nozzle diameter, $a \approx 1/2$, $b \approx n - 1$, and n is the cluster size.¹⁷ Clustering of rare gases also increases with atomic mass and decreases with nozzle temperature.¹⁸ Because the terminal Mach number varies as $(dP)^c$, where $c \approx 0.5$ for atoms,¹⁹ reducing either d or P increases the translational temperature. Although all of the rare gases have been used in interferometry experiments to produce cold beams of alkali atoms,¹⁵ reheating of the beam by cluster formation in Xe was problematic.^{16,20} Elsewhere, the flux of Xe was clusters reduced to less than 1% of the monomer by operating with $P < 1$ atm and $d < 0.1$ mm.²¹

Alternatively, the fraction of clusters may be reduced by either reducing m_c or increasing T_0 , both of which would increase the focal distance of the molecular beam [see Eq. (14)]. This effect can in turn be countered by increasing I_0 . Optimum conditions are likely to be achieved using Kr instead of Xe with a room temperature nozzle and a 60% increase in laser intensity.

The laser power required to focus the molecular beam depends on the desired focal distance and feature width. For the purpose of discussion we will choose an upper bound of 10 cm for the focal distances and 50 nm for the focal width. Using I_2 in Kr for illustration, and ignoring the effect of rotational temperature (which is absent for atoms and isotropic molecules), we may achieve these goals with a circular Gaussian (or the equivalent Bessel) beam having $\omega_0 = 30 \mu\text{m}$ and $I_0 = 1.6 \times 10^8 \text{ W/cm}^2$, which corresponds to a cw laser power of 2.2 KW. At an intersection angle of $\delta = 5^\circ$, the focal coordinates are $x_f = 9.2$ cm and $z_f = 0.8$ cm (see Fig. 3). The requisite power could be lowered by further reducing δ . A lower bound on δ is given by the requirement that the incidence angle be at least twice the divergence angle of the laser beam, which is 0.6° for $\omega_0 = 30 \mu\text{m}$ and $\lambda = 1.06 \mu\text{m}$. At grazing incidence, x_f grows approximately linearly with δ , whereas z_f grows faster than linearly, and both focal distances vary inversely with intensity. Thus, for example, at $\delta = 3^\circ$ and a power of 1.6 KW, the molecular beam focus is at $x_f = 10.0$ cm and $z_f = 0.5$ cm.

Although diode-pumped, solid-state cw lasers with output powers at the KW level have now been developed in the near infrared,²² the required powerful and high-spatial-quality radiation could be most readily accessed inside a laser resonator. Specifically, a 100 W solid-state laser employing a typical 10% output coupler²³ will have a total power of ~ 2 KW at any point in the cavity (i.e., twice the ~ 1 KW intracavity power propagating in each direction). Thus, by incorporating a suitable focusing section (with a $30 \mu\text{m}$ spot size) intersecting the molecular beam within the laser cavity (see Fig. 8),²⁴ a relatively modest (nominally 100 W) laser will suffice for the lithography radiation source.

Precise focusing of KW-level intracavity cw laser radiation at grazing incidence to an $\sim 10 \mu\text{m}$ -diameter molecular beam possesses several additional challenges. In particular, laser beam-pointing instabilities must be reduced to less than 10 nm at the intracavity focus to maintain the integrity of a high-quality, sub-100 nm molecular focus. This means that (i) the laser resonator must be operated at its most stable point (i.e., near the center of a cavity stability region), (ii) the

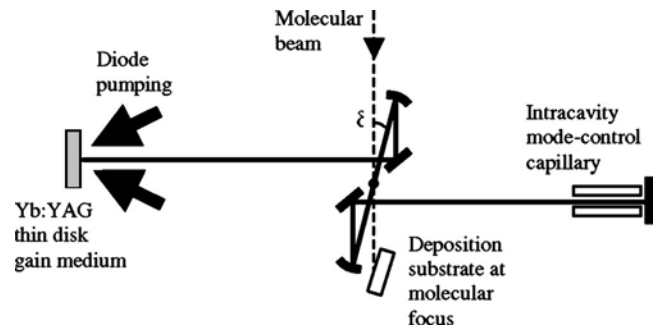


FIG. 8. Schematic drawing of the interaction region of the lithography apparatus.

resonator must be designed to minimize susceptibility to thermal effects, and (iii) the directionality of the intracavity laser radiation must be *very* well controlled. The first two criteria strongly suggest the use of a properly configured diode-pumped thin-disk laser resonator, such as a TEM_{00} -mode Yb:yttrium-aluminum-garnet (YAG) thin-disk laser.²⁵ The thin-disk laser geometry is relatively insensitive to thermal effects in the gain medium because thermal diffusion is predominantly parallel to the optical axis of the resonator.

Satisfying the third criterion is much more challenging. If we assume the use of a Yb:YAG thin-disk laser, then the properties of Yb:YAG (saturation of the ground-state absorption in a multi-pass pumping scheme, etc.³) imply a ~ 1 mm fundamental mode spot size (half width at e^{-1} of the field) at the gain medium. As a result, a focusing element with a focal length of about 10 cm will be needed to generate the required $30 \mu\text{m}$ spot size at the intracavity focus. The requirement to reduce beam-pointing instabilities at the focus to less than 10 nm implies that fluctuations in the directionality of the intracavity radiation must be less than $0.1 \mu\text{rad}$. It should be possible to satisfy this rather demanding performance specification by inserting a capillary,²⁶ rather than a simple aperture, in the cavity and by employing active feedback stabilization of the laser cavity. In addition to defining the optical axis of the laser resonator, a properly inserted intracavity capillary will force the spatial oscillation mode of the laser to match an HE_{mn} capillary mode. As shown by the analysis of Sec. III C, the cylindrically symmetric fundamental HE_{11} mode, which is represented by the $J_0(r)$ Bessel function truncated at the first minimum (the capillary radius), produces a molecular beam focus that is very similar to a TEM_{00} mode Gaussian spatial profile.

V. CONCLUSIONS

We have shown that intense-laser-based molecular optics can serve as a route to nanoscale processing of substrates with unique advantages. Because all atoms and molecules are polarizable, it is possible to manipulate any species that could be entrained in a molecular beam, including metals, insulators, semiconductors, and biomolecules. Complex, multi-material patterns could be made by using this technique for direct writing on the substrate. For continuous laser and molecular beams, the contrast ratio is expected to be far superior to that achieved with other state-of-the-art tech-

niques. Because the method is not diffraction limited by the optical wavelength, features <10 nm wide could be made with sufficient laser intensity. Finally, the method could be extended in principle to deposit aligned molecules, thereby creating nanostructures with anticipated new electric and optical properties.

The analysis in Sec. III shows that in the large- R limit the focal coordinates of the molecular beam, x_f and z_f , scale as $m\omega_0 T_0/m_c \alpha_{\parallel} I_0$, and W scales as W_i/ω_0^2 , where m is the mass of the deposited molecule, m_c is the mass of the carrier gas, T_0 is the source temperature, α_{\parallel} is the parallel component of the polarizability, I_0 is the peak laser intensity, W_i is the width of the molecular beam before focusing, and ω_0 is the e^{-1} radius of the electric field. Generally we wish to select physical conditions that minimize both of these ratios.

Because the focusing properties of a molecular lens scale as the ratio of the kinetic energy to the laser intensity, it is possible to reduce the requisite laser power by lowering the speed of the molecular beam. One way to reduce the speed is to seed the molecule of interest in a heavy carrier gas (i.e., by increasing m_c). An important finding in this article is that it is sufficient to reduce only the component of the velocity transverse to the laser beam, which may be accomplished rather simply by intersecting the laser and molecular beams at grazing incidence. At incidence angles on the order of $\delta = 5^\circ$, the requisite laser power is reduced to the point that presently available continuous-wave lasers could be used. A further benefit of using a grazing incidence is that the length of the deposited structure varies as $1/\sin \delta$, enabling the production of nanowires $>100 \mu\text{m}$ long.

The advantages of using cw rather than pulsed lasers for molecular lithography are the vastly increased duty cycle and the suppression of background molecules when the laser is off. An additional order-of-magnitude reduction in laser power may be achieved by having the laser and molecular beams intersect inside the laser cavity. A capillary waveguide serves the dual purpose of improving the pointing stability of the laser and eliminating unwanted transverse modes. Using realistic physical parameters, we estimate that it should be possible to produce 50-nm-wide structures with atoms and isotropic molecules and 200 nm features with anisotropic molecules with a 100 W laser. With ten times greater laser power it is possible to increase its spot size so as to reduce the feature width by a factor of 4.6 and to increase its length by 3.2, while maintaining the same focal distance.

The calculations reported here were performed using I_2 as a prototypical molecule. The method is completely general, however, and may be applied to any species that can be entrained in a molecular beam. With pulsed lasers there is not much advantage in using highly polarizable species because the ionization potential generally increases with polarizability, setting an upper bound on the intensity that could be used to deflect the molecules. The much lower intensity of a cw source, however, allows one to make full use of the enhanced polarizability of some species. From the scaling relations we find, for example, that Cs atoms require 6.7 times lower intensity than I_2 to reach the same focal distance. Metal clusters with small m/α_{\parallel} ratios may also be attractive candidates.

ACKNOWLEDGMENTS

Support by the Chemical Sciences, Geosciences and Biosciences Division of the Office of Basic Energy Sciences, Office of Science, U.S. Department of Energy is gratefully acknowledged. The authors also wish to thank the Motorola Advanced Technology Center in Schaumburg, Illinois for co-sponsoring this project through the Illinois Manufacturing Research Center.

- ¹T. Seideman, Phys. Rev. A **56**, R17 (1997).
- ²T. Seideman, J. Chem. Phys. **106**, 2881 (1997).
- ³T. Seideman, J. Chem. Phys. **107**, 10420 (1997).
- ⁴Z.-C. Yan and T. Seideman, J. Chem. Phys. **111**, 4113 (1999).
- ⁵T. Seideman, J. Chem. Phys. **111**, 4397 (1999).
- ⁶H. Stapelfeldt, H. Sakai, H. E. Constant, and P. B. Corkum, Phys. Rev. Lett. **79**, 2787 (1997).
- ⁷H. Sakai, A. Tarasevitch, J. Danilov, H. Stapelfeldt, R. W. Yip, C. Ellert, E. Constant, and P. B. Corkum, Phys. Rev. A **57**, 2794 (1998).
- ⁸B. S. Zhao, H. S. Chung, K. Cho, S. H. Lee, S. Hwang, J. Yu, Y. H. Ahn, J. Y. Sohn, D. S. Kim, W. K. Kang, and D. S. Chung, Phys. Rev. Lett. **85**, 2705 (2000).
- ⁹H. S. Chung, B. S. Zhao, S. H. Lee, S. G. Hwang, K. C. Cho, S. H. Shim, S. M. Lim, W. K. Kang, and D. S. Chung, J. Chem. Phys. **114**, 8293 (2001).
- ¹⁰See, for example, K. S. Johnson, J. H. Thywissen, N. H. Dekker, K. K. Berggren, A. P. Chu, R. Younkin, and M. Prentiss, Science (Washington, DC) **280**, 1583 (1998).
- ¹¹A. Yariv, Quantum Electronics, 3rd ed. (Wiley, New York, 1989), Chap. 6.
- ¹²S. DePaul, D. Pullman, and B. Friedrich, J. Phys. Chem. **97**, 2167 (1993).
- ¹³A. N. Chester and R. L. Abrams, Appl. Phys. Lett. **21**, 576 (1972); R. L. Abrams and A. N. Chester, Appl. Opt. **13**, 2117 (1974); F. P. Roullard and M. Bass, IEEE J. Quantum Electron. **QE-13**, 813 (1977).
- ¹⁴In these calculations we ignored the divergence of the laser beam. The justification for this simplification is that, in this focusing regime, divergence has no measurable effect on the focusing properties of a Gaussian beam.
- ¹⁵J. Schmeidmayer, M. S. Chapman, C. R. Ekstrom, T. D. Hammond, D. A. Kokorowski, A. Lenef, A. Rubenstein, E. T. Smith, and D. E. Pritchard, Atom Interferometry, edited by P. A. Berman (Academic, San Diego, CA, 1997), pp. 2–83.
- ¹⁶The brightness, defined as the flux per unit area of the molecular beam skimmer, is quoted as $10^{21} \text{sr}^{-1} \text{cm}^{-2} \text{s}^{-1}$, which corresponds to a flux of $10^{18} \text{sr}^{-1} \text{s}^{-1}$ (D. Pritchard, private communication).
- ¹⁷U. Buck and H. Meyer, Surf. Sci. **156**, 275 (1985).
- ¹⁸O. F. Hagena and W. Obert, J. Chem. Phys. **56**, 1793 (1972).
- ¹⁹D. R. Miller, in Atomic and Molecular Beam Methods, edited by G. Scoles (Oxford, New York, 1988), Vol. I, pp. 15–53.
- ²⁰Note that cluster formation within the focus of the molecular beam is negligible. The flux of carrier atoms at a distance d is Φ/d^2 , the number density is $n = \Phi/vd^2$, and the number density in the focal volume is $n_f = nW_i/W$. Assuming $\Phi = 10^{19} \text{sr}^{-1} \text{s}^{-1}$, $v = 300 \text{m s}^{-1}$, $W_i = 10 \mu\text{m}$, and $W = 50 \text{nm}$, we estimate $n_f = 2 \times 10^{11} \text{cm}^{-3}$ and the interatomic distance is 530 nm.
- ²¹R. Thissen, P. Lablanquie, R. I. Hall, M. Ukai, and K. Ito, Eur. Phys. J. D **4**, 335 (1998).
- ²²C. Stewen, K. Contag, M. Larionov, A. Giesen, and H. Hügel, IEEE J. Sel. Top. Quantum Electron. **6**, 650 (2000).
- ²³W. Koechner, Solid-State Laser Engineering, 5th ed., Springer Series in the Optical Sciences (Springer, New York, 1999).
- ²⁴S. T. Lee, G. McConnell, A. Major, N. Langford, and A. I. Ferguson, paper CWF4, p. 335, technical digest of the Conference on Lasers and Electro-Optics (CLEO) 2001 (Optical Society of America, Washington, DC, 2001), Paper CWF4, p. 335.
- ²⁵A commercial laser encompassing the thin-disk design and generating up to 100 W of output power in the fundamental TEM₀₀ spatial mode ($M^2 < 1.1$) is now also available (see www.versadisk.com).
- ²⁶A. N. Chester and R. L. Abrams, Appl. Phys. Lett. **21**, 576 (1972); R. L. Abrams and A. N. Chester, Appl. Opt. **13**, 2117 (1974); F. P. Roullard and M. Bass, IEEE J. Quantum Electron. **QE-13**, 813 (1977).